

Electronic Annex

Structure and reactivity of oxalate surface complexes on lepidocrocite derived from infrared spectroscopy, DFT-calculations, adsorption, dissolution and photochemical experiments

Susan C. Borowski^a, Jagannath Biswakarma^{a,c}, Kyounglim Kang^b, Walter D.C. Schenkeveld^b, Janet G. Hering^{a,c,d}, James D. Kubicki^e, Stephan M. Kraemer^b, Stephan J. Hug^{a*}

^a Eawag, Swiss Federal Institute of Aquatic Science and Technology, Ueberlandstrasse 133, CH-8600 Duebendorf, Switzerland

^b University of Vienna, Dept. of Environmental Geosciences and Environmental Science Research Network, Althanstraße 14 (UZA II) 1090 Vienna, Austria

^c Swiss Federal Institute of Technology (ETH) Zürich, IBP, CH-8092 Zürich, Switzerland

^d Swiss Federal Institute of Technology Lausanne (EPFL), ENAC, CH-1015 Lausanne, Switzerland

^e The University of Texas at El Paso, Dept. of Geological Sciences, 500 West University Avenue, El Paso, TX 79968, USA

* Corresponding author. E-mail: stephan.Hug@eawag.ch

Current address of S.C. Borowski: Virginia Military Institute, Lexington, VA 24450, USA. E-mail: borowskisc@vmi.edu

CONTENTS

Table EA1.	Comparison of experimental and theoretical IR frequencies.	3
Table EA2.	Gaussian fit parameters for spectra measured at various pH values in H ₂ O and in D ₂ O at pH 4-5.	3
Table EA3.	Peak positions of Gaussians for individual fits of spectra and for simultaneous fits.	4
Table EA4.	Comparison of average bond distances, angles, and dihedral angles.	5
Table EA5.	Experimental and calculated IR and Raman frequencies of aqueous oxalic acid, oxalate dianion, and trisoxalatoiron(III).	5
Table EA6.	Comparison of average bond distances, angles; periodic cells and molecular clusters.	6
Table EA7.	Comparison of experimental and theoretical IR frequencies of inner sphere bonding geometries of oxalate to lepidocrocite.	7
Table EA8A.	Atomic Valences and Mayer Atomic Bond orders of BTri , BM , and MM .	8
Table EA8B.	Natural Population analysis of BTri , BM , and MM .	8
Table EA9.	Comparison of experimental and theoretical IR frequencies.	9
Figure EA1.	ATR-FTIR spectra of Lp-1 lepidocrocite, difference spectra during CO ₂ desorption, and spectra of adsorbed oxalate as a function of time and pH on Lp-1 and Lp-2 .	10
Figure EA2.	Fe mobilization from Lp-2 lepidocrocite by oxalate at different pH values.	11
Figure EA3.	SVD-Analysis of spectra from adsorption of aqueous oxalate on Lp-1 .	12
Figure EA4.	SVD-Analysis of spectra from adsorption of aqueous oxalate on Lp-2 .	13
Figure EA5.	Spectra of adsorbed oxalate on lepidocrocite at pH 4.0 and Gaussian fits.	14
Figure EA6.	Adsorption of oxalic acid on Lp-1 as a function of pH and spectral fits	15
Figure EA7.	Range of peak positions from Gaussian fits to different datasets and subsets.	16
Figure EA8.	Molecular clusters of oxalic acid, oxalate and trisoxalatoiron(III).	16
Figure EA9.	Linear regression plots that compare experimental and theoretical frequencies of aqueous oxalic acid, oxalate dianion, and oxalatoiron(III).	17
Figure EA10.	Geometry-optimized molecular clusters of oxalate adsorbed to lepidocrocite.	18
Figure EA11.	Geometry-optimized molecular clusters of solvated lepidocrocite cluster [Fe ₈ O ₃₈ H ₅₄] ²⁺ , representing (010) and (100) surfaces.	19
Figure EA12.	Linear regression comparison of experimental and theoretical frequencies of molecular clusters modeling inner-sphere bonded complexes.	20
Figure EA13.	Geometry-optimized molecular cluster with protonated BM .	21
Figure EA14.	Geometry-optimized molecular cluster H-OS₍₀₁₀₎ and H-OS₍₁₀₀₎ .	22
Figure EA15.	Linear regression comparison of experimental and theoretical frequencies of H-OS₍₀₁₀₎ and H-OS₍₁₀₀₎ .	22
References		23

Table EA1. Comparisons of experimental and theoretical IR frequencies (cm^{-1}) of **BM** with and without the PCM method.^{a,b}

modes	experimental frequencies	theoretical frequencies	
		No PCM	PCM=(water)
$v_s(\text{C}-\text{O})$	1275 ± 6	1281 (6)	1276 (1)
$v_s(\text{C}-\text{O})$	1286 ± 4	-	-
$v_a(\text{C}-\text{O})$	1308 ± 1	-	-
$v_a(\text{C}-\text{O})$	1403 ± 4	1406 (3)	1402 (-1)
$v_a(\text{C}-\text{O})$	1422 ± 4	-	-
$v_a(\text{C}-\text{O})$	1567 ± 7	-	-
$v_a(\text{C}=\text{O})$	1609 ± 18	-	-
$v_a(\text{C}=\text{O})$	1641 ± 28	1632 (-9)	1590 (-51)
$v_a(\text{C}=\text{O})$	1664 ± 9	-	-
$v_a(\text{C}=\text{O})$	1684 ± 3	1683 (-1)	1680 (-4)
$v_a(\text{C}=\text{O})$	1712 ± 1	1698 (-14)	-
		R^2	0.999
		slope	0.959
		y-intercept	59.787
		average difference	7
			14

^aDifferences between experimental and theoretical frequencies are given in parentheses.

^bGaussian peaks assigned to S_{BM} are in red, Gaussian peaks assigned to S_{MM} are in blue, and Gaussian peaks assigned to S_{OS} are in green.

Table EA2. Gaussian fit parameters for spectra measured at various pH values in H₂O and in D₂O at pH 4-5

Gaussian	peak positions										average (\pm stdev)	pD = 4-5
	pH = 4.0	4.5	5.0	5.5	6.0	6.5	7.0	8.0	9.0			
1	1269	1272	1268	1273	1277	1280	1276	1273	1276	1274 ± 4	1270 (-2)	
2	1287	1298	1290	1289	1291	1289	1290	1290	1293	1291 ± 3	1299 (1)	
3	1308	1308	1309	1308	1308	1308	1308	1308	1308	1308	1312 (4)	
4	1405	1407	1398	1404	1403	1402	1402	1407	1407	1404 ± 3	1406 (-1)	
5	1425	1425	1425	1425	1428	1429	1430	1433	1433	1428 ± 3	1440 (15)	
6	1566	1566	1566	1566	1566	1566	1566	1566	1566	1566	1564 (-2)	
7	1595	1595	1595	1595	1595	1596	1599	1595	1595	1596 ± 1	1597 (2)	
8	1626	1628	1624	1624	1625	1626	1622	1622	1622	1624 ± 2	1626 (-2)	
9	1658	1659	1656	1657	1655	1654	1652	1650	1650	1655 ± 3	1654 (-5)	
10	1685	1684	1683	1682	1679	1677	1677	1682	1682	1681 ± 3	1680 (-4)	
11	1713	1711	1711	1712	1710	1707	1709	1709	1709	1710 ± 2	1710 (-1)	

Three species were assumed: red, blue, and green.

*Differences between peak positions at pH = 4.5 in H₂O and pD 4-5 in D₂O are given in parentheses.

Table EA3. Peak positions of Gaussians for individual fits of spectra and for simultaneous fits.

The numbers in columns pH 3.0-6.0 are the parameters for Gaussians fitted to the spectra at each pH individually. The numbers in columns pH, kinetic and pH & kinetic are parameters for Gaussians that fit all spectra simultaneously (stable equilibrium spectra for Lp-1, spectra at all times and pH values for Lp-2, and for both data sets combined).

		S _{BM}								
		pH 3.0	pH 4.0	pH 5.5	pH 6.0	pH ¹	kinetic	pH & kinetic ²	Aver.	Stdev.
Peak 1	Peak max.	1269	1269	1273	1276	1277	1274	1286	1275	6
	Width	55	50	41	40	83	28	87		
	Area	3233	2012	1032	522	2012				
Peak 2	Peak max.	1403	1405	1403	1403	1401	1407	1395	1403	4
	Width	60	52	48	40	53	71	55		
	Area	3436	2838	1016	729	2814	2862	3216		
Peak 3	Peak max.	1625	1626	1624	1625	1647	1700	1640	1641	28
	Width	38	45	39	37	105	59	104		
	Area	5305.5	4728.4	3628.3	2786.8	2383.9	2711.1	2929.3		
Peak 4	Peak max.	1684	1684	1681	1679	1687	1688	1685	1684	3
	Width	28	31	31	29	24	29	25		
	Area	7723	8103	4516	3094	4496	6298	5236		
Peak 5	Peak max.	1712	1712	1711	1709	1712	1712	1711	1712	1
	Width	30	23	20	27	23	16	21		
	Area	6024	3920	1196	710	4801	4505	5176		

		S _{MM}								
		pH 3.0	pH 4.0	pH 5.5	pH 6.0	pH ¹	kinetic	pH & kinetic ²	Ave.	Stdev.
Peak 1	Peak max.	1287	1287	1287	1290	1286	1282	1280	1286	4
	Width	55.0	55.0	55.0	47.4	55.7	66.6	40.9		
	Area	1390	1656	1656	917	1656				
Peak 2	Peak max.	1420	1424	1424	1428	1421	1417	1420	1422	4
	Width	57.1	46.0	46.0	38.9	44.7	47.2	45.3		
	Area	1947	2225	2225	1541	2821	2483	2701.3		
Peak 3	Peak max.	1595	1595	1595	1595	1632	1632	1616	1609	18
	Width	55.0	55.0	55.0	40.6	75.4	59.4	67.7		
	Area	1496	2447	2447	1393	4931	4160	4539		
Peak 4	Peak max.	1658	1658	1658	1655	1673	1673	1673	1664	9
	Width	35.8	35.3	35.3	33.7	41.6	38.4	40.4		
	Area	6701	5643	5643	3739	4632	5701	5061		

		S _{OS}								
		pH 3.0	pH 4.0	pH 5.5	pH 6.0	pH ¹	kinetic	pH & kinetic ²	Ave.	Stdev.
Peak 1	Peak max.	1308	1308	1308	1308	1309	1307	1309	1308	1
	Width	20.0	20.0	20.0	15.0	9.3	19.3	22.7		
	Area	2074	1536	1536	454	1536				
Peak 2	Peak max.	1566	1566	1566	1566	1560	1581	1564	1567	7
	Width	40.0	40.0	40.0	40.0	62.7	73.0	71.3		
	Area	691	860	860	690	2231	1379	1251		

¹ Spectral fits for Lp-1, pH-dependence, shown in Figure EA6.

² spectral fits for Lp-2, pH and kinetics, shown in Figure 5.

Table EA4. Comparison of average bond distances^a, angles^b, and dihedral angles^b of experimental (expt) and calculated (calc.) oxalic acid and trioxalatoiron(III).

	oxalic acid			trioxalatoiron(III)		
	ave. expt. ^c	calc.	Δ	ave. expt. ^d	calc.	Δ
bonds^a						
C-C	1.546	1.564	0.018	1.544	1.563	0.019
O-Fe	-	-	-	2.009	2.017	0.007
FeO-C	-	-	-	1.337	1.530	0.193
O-C	1.213	1.222	0.009	1.226	1.238	0.013
HO-C	1.280	1.308	0.028	-	-	-
angles^b						
O-C-O	126.8	122.0	-4.8	125.6	125.7	0.2
O-C-C-O	-	-	-	175.4	174.8	0.2
dihedral angles^b						
HO-C-C-OH	179.7	179.4	-0.3	-	-	-
HO-C-C-O	0.2	0.7	0.5	-	-	-

^ain Å, ^bin degrees, ^c (Braga et al., 2002; Brill et al., 1943; Martin and Alan Pinkerton, 1998) ^d (Akutsu et al., 2004; Coronado et al., 2006; Saritha et al., 2012)

Table EA5. Experimental and calculated IR and Raman frequencies (cm^{-1}) of aqueous oxalic acid, oxalate dianion, and trioxalatoiron(III).^a

	oxalic acid		oxalate dianion		trioxalatoiron(III)			
	Expt ^a	Calc. ^b	Expt ^c	Calc. ^d	Expt ^e	Calc. ^f		
$\nu_s(\text{C}-\text{O})$	1230	1244 (14)	$\nu_a(\text{C}-\text{O})$	1308	1286 (-22)	$\nu(\text{C}-\text{O})$	1250	1257 (7)
$\nu_s(\text{C}-\text{O})$	1447	1408 (-39)	$\nu_s(\text{C}-\text{O})$	1489	1453 (-36)	$\nu_{as}(\text{C}-\text{O})$	1266	1264 (-2)
$\nu_a(\text{C}=\text{O})$	1720	1717 (-3)	$\nu_a(\text{C}-\text{O})$	1570	1565 (-5)	$\nu(\text{C}-\text{C})$	1390	1365 (-25)
						$\delta(\text{H}_2\text{O})$	1649	1647 (-2)
						$\nu_{as}(\text{C}=\text{O})$	1679	1678 (+1)
						$\nu_s(\text{C}=\text{O})$	1712	1685 (-27)
R^2	0.988		0.989		0.996			
slope	0.973		1.040		0.988			
y-intercept	+30.076		-79.772		8.903			
stdev of error	27		16		13			

Differences between experimental and theoretical frequencies are given in parentheses.

a: (Shippey, 1980), b: $[\text{H}_2\text{C}_2\text{O}_4 \cdot 4 \text{ H}_2\text{O}]$, c: (Hind et al., 1998), d: $[\text{C}_2\text{O}_4 \cdot 4 \text{ H}_2\text{O}]^{2-}$, e: (Fujita et al., 1962), f: $[\text{Fe}(\text{C}_2\text{O}_4)_3 \cdot 12 \text{ H}_2\text{O}]^{3-}$. Range for oxalic acid: (Persson and Axe, 2005) and our data.

Table EA6. Comparison of average bond distances (\AA)^a, angles(degrees)^b, and dihedral angles^b of periodic cells (PC) and molecular clusters (MC).

BTetra ₁		BTetra ₂		BTri ₂		MB		BB ₁		BB ₂		BB ₂ [*]		BM ₁		BM ₂		MM		
PC	MC	PC	MC	PC	MC	PC	MC	PC	MC	PC	MC	PC	MC	PC	MC	PC	MC	PC	MC	
bonds^a																				
Fe-O	2.035	2.172	2.110	2.227	2.056	2.130	2.060	2.224	2.025	2.083	2.031	2.119	1.935	1.983	2.073	2.235	1.985	2.100	1.934	1.953
C-C	1.568	1.566	1.538	1.540	1.577	1.563	1.547	1.551	1.553	1.540	1.545	1.539	1.559	1.537	1.529	1.528	1.542	1.556	1.533	1.576
O-C	1.280	1.262	1.287	1.265	1.279	1.263	1.281	1.265	1.269	1.262	1.278	1.269	1.283	1.266	1.281	1.265	1.279	1.262	1.279	1.261
angles^b																				
O-C-O	129.5	127.7	122.9	124.9	125.8	125.5	126.6	125.9	123.9	127.2	127.6	126.0	120.4	125.0	122.3	124.5	123.7	125.5	123.2	124.5
C-C-O	115.2	116.1	118.4	117.5	117.0	117.3	116.7	117.0	118.0	116.4	116.2	116.9	119.8	117.5	118.7	117.7	118.2	117.2	118.4	117.8
approx. symmetry	D_{2h}	D_{2h}	D_{2d}	D_{2d}	D_{2h}	D_{2h}	D_{2d}	D_{2d}	D_{2d}	D_{2d}	D_{2d}	D_{2h}	D_{2d}	D_{2d}	D_{2d}	D_{2h}	D_{2h}	D_{2d}	D_{2h}	

Note that the DFT methods are different (PBE for periodic vs B3LYP for clusters).

Table EA7. Comparisons of experimental and theoretical IR frequencies (cm^{-1}) of inner-sphere bonding geometries of oxalate to lepidocrocite for molecular clusters - $\text{C}_2\text{H}_{54}\text{O}_{42}\text{Fe}_8$.^{a,b}

modes	experimental frequencies	theoretical frequencies							
		BTetra ₁	BTetra ₂	MB	BB'	BB	BB ₂ *	BM'	
$\nu_s(\text{C}-\text{O})$	1275 ± 6	1291 (16)	1272 (-3)	-	-	1159 (-116)	1217 (-58)	-	
$\nu_s(\text{C}-\text{O})$	1286 ± 4	-	-	1272 (-14)	1297 (11)	-	-	1304 (18)	
$\nu_a(\text{C}-\text{O})$	1308 ± 1	-	-	-	-	-	-	-	
$\nu_a(\text{C}-\text{O})$	1403 ± 4	1398 (-5)	1426 (23)	-	-	1319 (-84)	1370 (-33)	-	
$\nu_a(\text{C}-\text{O})$	1422 ± 4	-	-	1414 (-8)	1440 (18)	-	-	1478 (56)	
$\nu_a(\text{C}-\text{O})$	-	-	-	-	-	-	-	1513	
$\nu_a(\text{C}=\text{O})$	1567 ± 7	-	-	-	-	-	-	-	
$\nu_a(\text{C}=\text{O})$	-	-	1569	1574	-	-	-	-	
$\nu_a(\text{C}=\text{O})$	1609 ± 18	-	-	1586 (-23)	1593 (-16)	-	-	1612 (3)	
$\nu_a(\text{C}=\text{O})$	1641 ± 28	1611 (-30)	1598 (-43)	-	-	missing	1626 (-17)	-	
$\nu_a(\text{C}=\text{O})$	1664 ± 9	-	-	missing	1621 (-43)	-	-	1692 (28)	
$\nu_s(\text{C}-\text{O})$	1684 ± 3	1624 (-60)	1648 (-36)	-	-	1692 (8)	1672 (-12)	-	
$\nu_s(\text{C}-\text{O})$	1712 ± 1	1685 (-27)	1694 (-18)	-	-	1719 (7)	1692 (-20)	-	
		R^2	0.994	0.989	0.999	0.993	0.9997	0.999	0.983
		slope	0.866	0.899	0.962	0.856	1.293	1.086	0.965
		y-intercept	185.816	139.733	39.542	207.761	-490.863	-160.594	78.819
		average difference	28	25	16	23	63	28	26

^aDifferences between experimental and theoretical frequencies are given in parentheses.

^bGaussian peaks assigned to S_{BM} are in red, Gaussian peaks assigned to S_{MM} are in blue, and Gaussian peaks assigned to S_{OS} are in green.

Table EA8A. Atomic Valences and Mayer Atomic Bond orders of **BTri**, **BM**, and **MM**.

	BTri	BM	MM
O ₁	1.8	1.84	1.83
O ₂	1.8	1.80	1.81
O ₃	2.0	1.91	1.91
O ₄	1.9	1.90	1.88
C ₁	3.7	3.7	3.7
C ₂	3.8	3.8	3.9
Fe ₁	2.2	2.2	2.0
Fe ₂	2.6	-	-

Table EA8B. Natural Population analysis of **BTri**, **BM**, and **MM**.

	BTri	BM	MM
O ₁	-0.34	-0.34	-0.34
O ₂	-0.36	-0.35	-0.40
O ₃	-0.32	-0.34	-0.35
O ₄	-0.35	-0.35	-0.36
C ₁	0.39	0.37	0.38
C ₂	0.37	0.37	0.37
Fe ₁	2.94	2.98	3.00
Fe ₂	2.92	-	-

Table EA9. Comparisons of experimental and theoretical IR frequencies (cm^{-1}) of inner-sphere bonding geometries of BM-H^+ , $\text{C}_2\text{H}_{55}\text{O}_{42}\text{Fe}_{8+}$.^{a,b}

modes	experimental frequencies	theoretical frequencies
$\nu_s(\text{C-O})$	1275 \pm 6	1314 (39)
$\nu_s(\text{C-O})$	1286 \pm 4	-
$\nu_a(\text{C-O})$	1308 \pm 0	-
$\nu_a(\text{C-O})$	1403 \pm 4	1400 (-3)
$\nu_a(\text{C-O})$	1422 \pm 4	-
$\nu_a(\text{C=O})$	1569 \pm 7	-
$\nu_a(\text{C=O})$	1609 \pm 18	-
$\nu_a(\text{C=O})$	1641 \pm 28	missing
$\nu_a(\text{C=O})$	1664 \pm 9	-
$\nu_s(\text{C-O})$	1684 \pm 3	1680 (-4)
$\nu_s(\text{C-O})$	1712 \pm 1	1765 (47)
<i>R</i> ²		0.981
slope		1.001
y-intercept		20.080
average difference		23

^aDifferences between experimental and theoretical frequencies are given in parentheses.

^bGaussian peaks assigned to S_{BM} are in red, Gaussian peaks assigned to S_{MM} are in blue, and Gaussian peaks assigned to S_{OS} are in green.

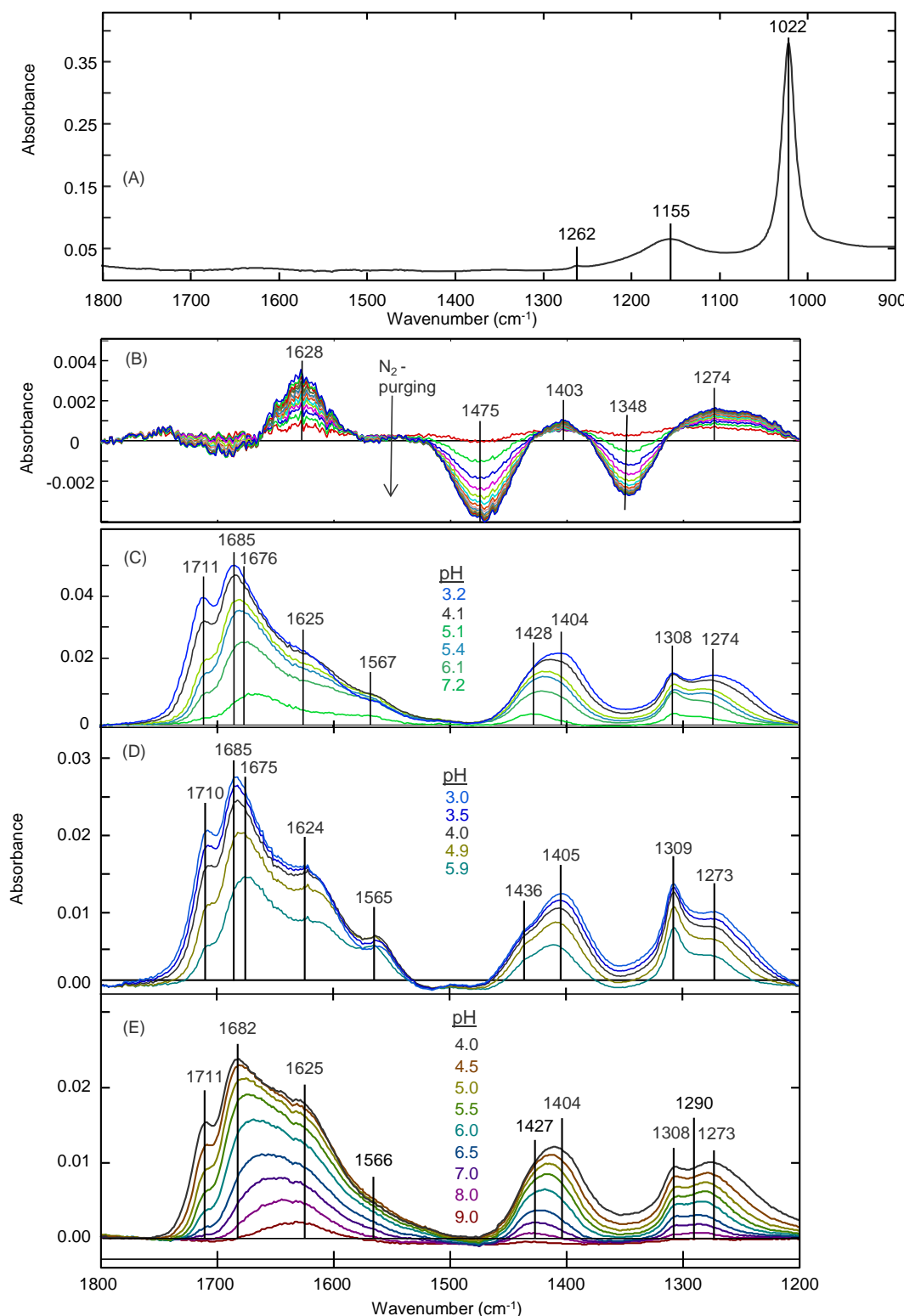


Figure EA1. (A) ATR-FTIR spectra of lepidocrocite (**Lp-1**). Vibrations at 1155 and 1022 cm⁻¹ are attributed to in-plane bending $\delta(\text{OH})$. (Cornell and Schwertmann, 2003). (B) difference spectra collected during CO₂ desorption during purging of the solution with N₂. (C) Adsorption of aqueous oxalate (200 μM , $I=10 \text{ mM KCl}$) on **Lp-1** and (D) of Lp-2 at various pH values, spectra recorded close to equilibrium (same as Figures 2A and 2B in main paper re-plotted here for comparison with the other spectra). (E) Spectra of adsorbed oxalate at different pH values after slow adjustment of pH with computer-controlled titrators (figure adapted from Hug and Bahnemann (Hug and Bahnemann, 2006)). All peak position agree to $\pm 3 \text{ cm}^{-1}$ or better. The shoulder at 1427–1436 cm⁻¹ cannot be as definitely located as the maxima and show some larger variation. The changes of the spectral shape with pH are closely the same for three measurements.

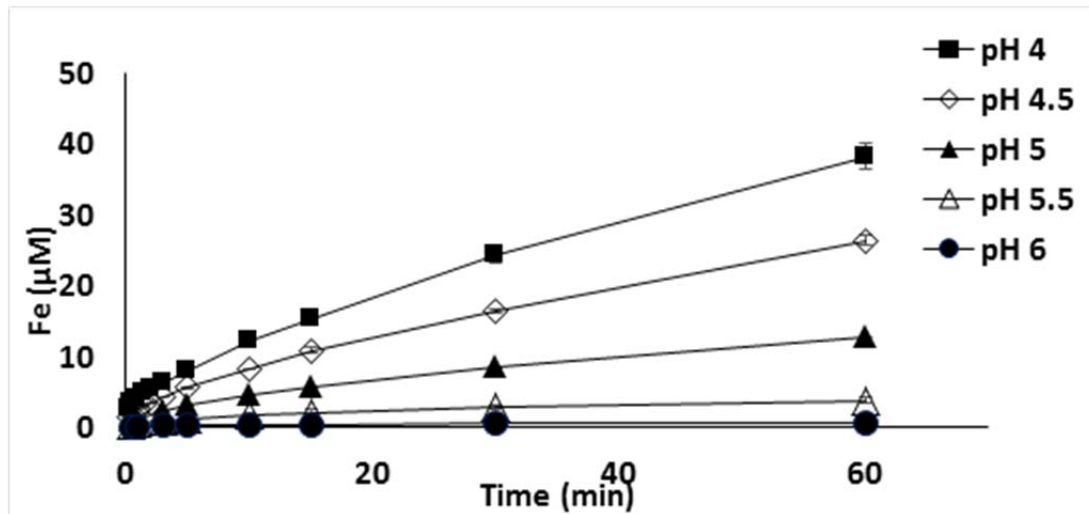


Figure EA2. Fe mobilization from Lp-2 lepidocrocite by oxalate at different pH values. The total oxalate concentration was 500 μM . 0.01 M NaCl solution was used as electrolyte. The solids concentrations was 0.1 g L^{-1} . Steady state rates of ligand controlled dissolution were calculated from the slopes by least squares fitting of a linear equation to the data between 0.5 and 5 minutes. Initial dissolution rates were used to remain far from equilibrium and to minimize the influence Fe-oxalate on oxalate adsorption.

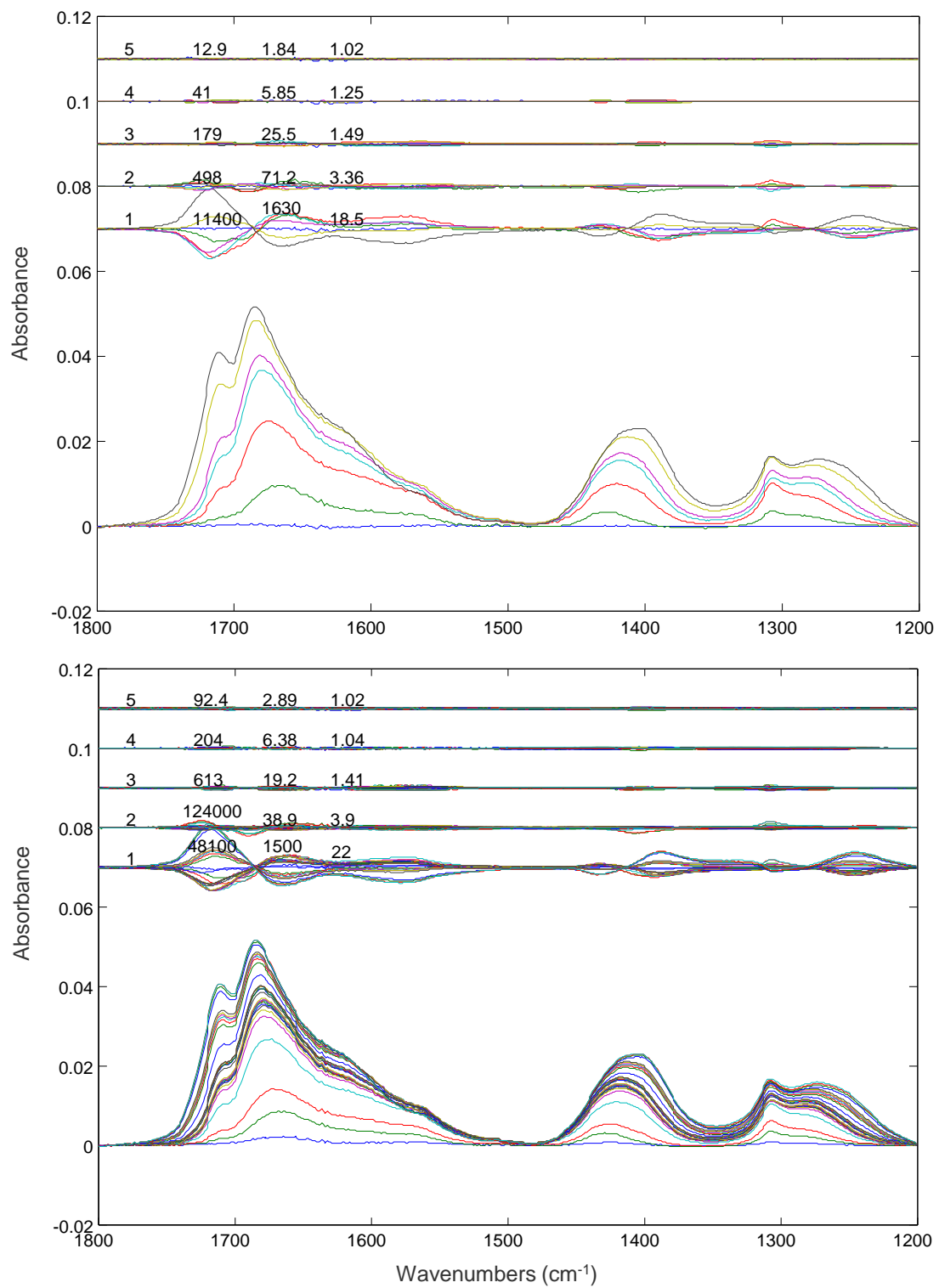


Figure EA3. SVD-Analysis of the spectra from adsorption of aqueous oxalate (200 μ M, $I= 10$ mM KCl) on **Lp-1** at various pH values. Top panel: Spectra close to equilibrium. Lower panel: Averages (from groups of 10 spectra each) of all 300-400 spectra collected during the experiment (30-40 averages). Shown are the spectra and the residuals (spectra-reproduced spectra) obtained by reproducing the spectra with increasing numbers of SVD-components. The residuals are shown offset above the spectra. The numbers noted above the residuals indicate the number of SVD-components, the sum of squared residuals (SSR), SSR/number of spectra, and the maximum value of SSR divided by the maximum value of the absorbance in the spectra in % (%Difference). Three components provide an adequate fit to the measured spectra. The SSR (calculated over the whole spectral range) still improves from 3-5 components, but the relative error (%Difference, which is calculated from the peak maxima) decreases strongly from 1-3 components, but much less with more than 3 components.

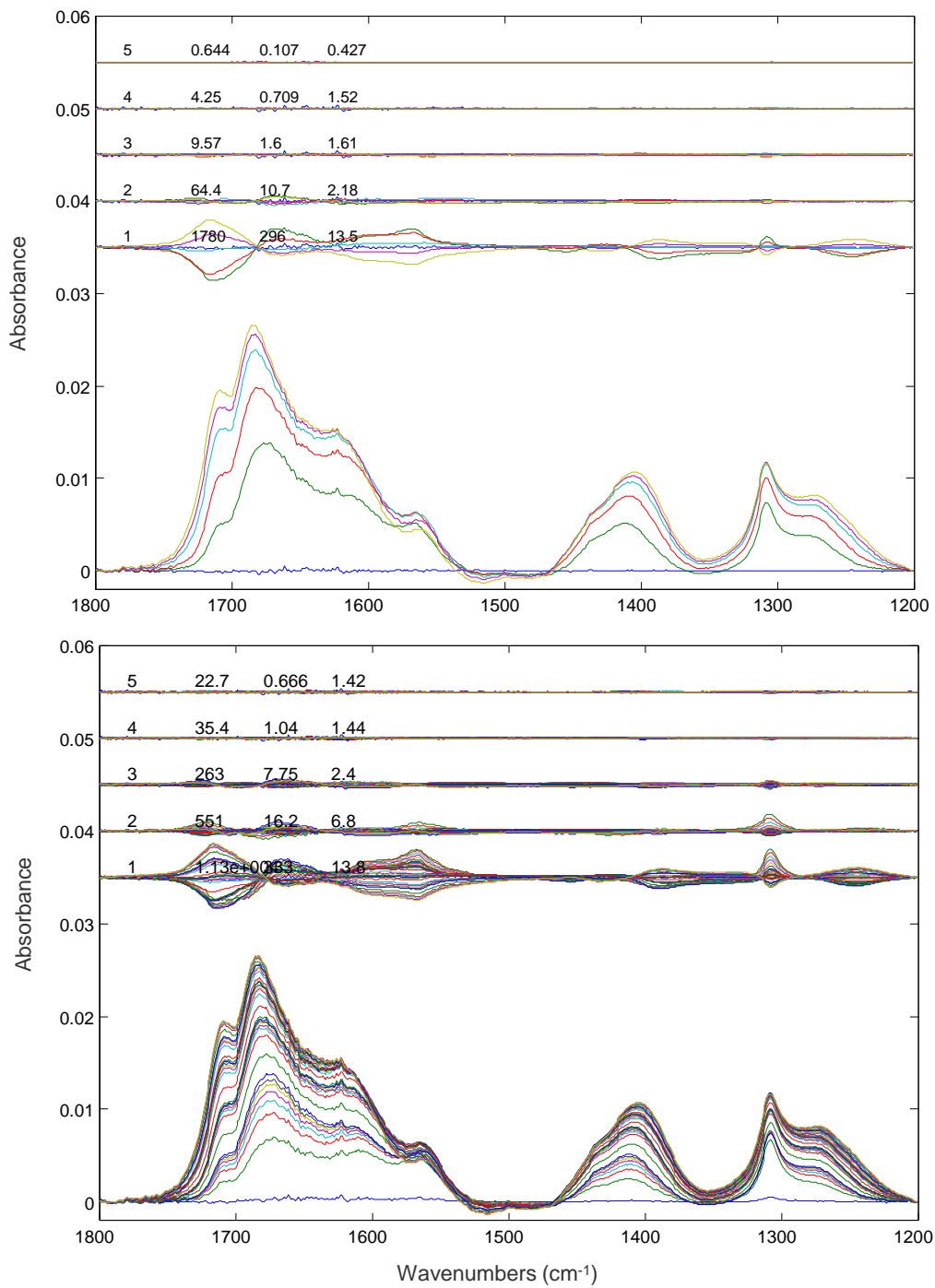


Figure EA4. SVD-Analysis of the spectra from adsorption of aqueous oxalate ($200 \mu\text{M}$, $I = 10 \text{ mM KCl}$) on **Lp-2** at various pH values. Top panel: Spectra close to equilibrium. Top panel: Averages (from groups of 10 spectra each) of all 300-400 spectra collected during the experiment (30-40 averages). Shown are the spectra and the residuals (spectra-reproduced spectra) obtained by reproducing the spectra with increasing numbers of SVD-components. The residuals are shown offset above the spectra. The numbers noted above the residuals indicate the number of SVD-components, the sum of squared residuals (SSR), SSR/number of spectra, and the maximum value of SSR divided by the maximum value of the absorbance in the spectra in % (%Difference). Three components provide an adequate fit to the measured spectra. The SSR (calculated over the whole spectral range) still improves from 3-5 components, but the relative error (%Difference, which is calculated from the peak maxima) decreases strongly from 1-3 components, but less with more than 3 components.

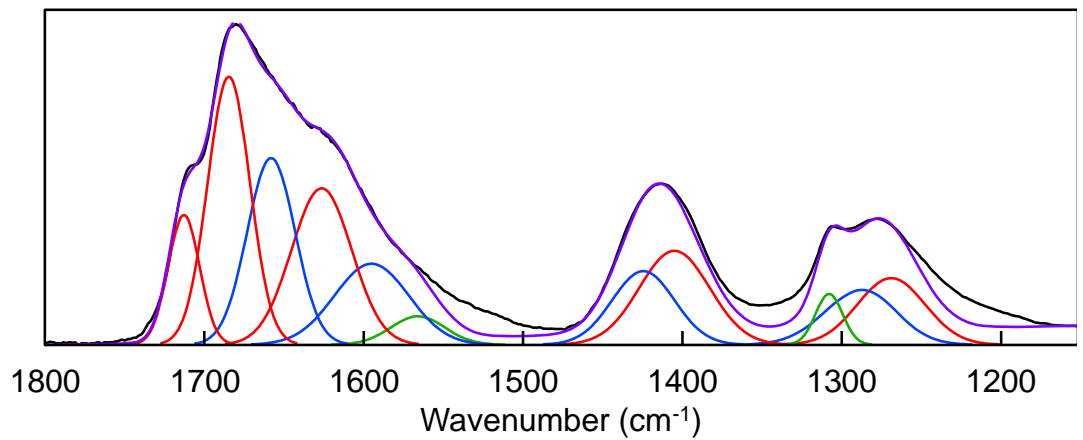


Figure EA5. Spectra of oxalate (200 μM , $I = 10 \text{ mM KCl}$) adsorbed on lepidocrocite at pH 4.0 (black line). Data fit with Gaussians peaks of three species (**BM**, **MM**, and **OS**), summation line in **purple**.

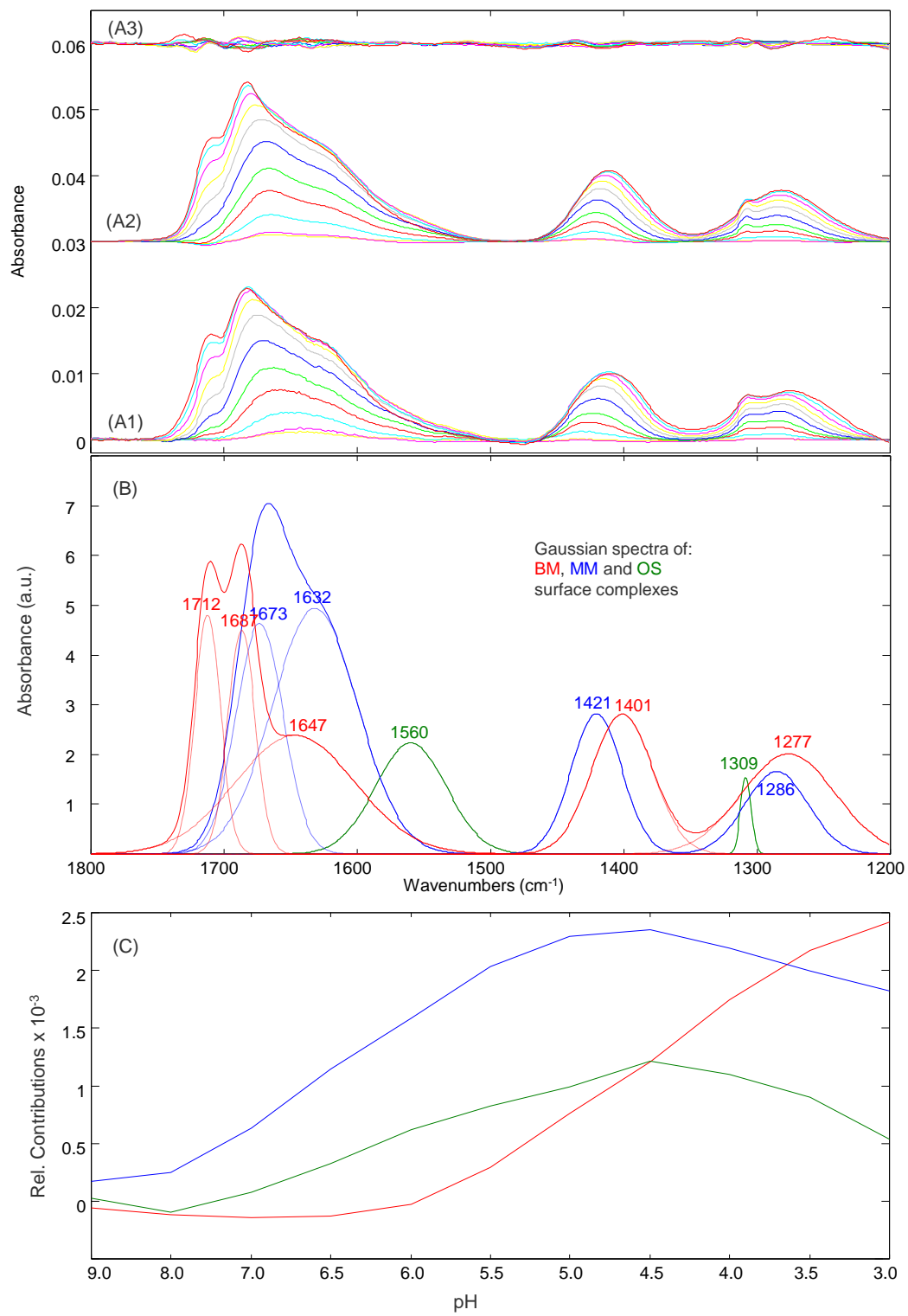


Figure EA6. Adsorption of oxalic acid (200 μM , I=10 mM NaCl) on **Lp-1** as a function of pH and spectral fits. (A1) Absorbance changes are the same as in Figure 2B as function of pH (more spectra are shown). (A2) reconstructed spectra with Gaussian line shapes (offset by 0.03 abs. units) and (A3) residuals (measured minus reconstructed spectra), offset by 0.06 abs. units). (B) Gaussian fits with five possible peaks for spectrum BM, four possible peaks for spectrum MM, and two possible peaks for spectrum OS. (C) Contributions of BM, MM, and OS Gaussian spectra as a function of pH.

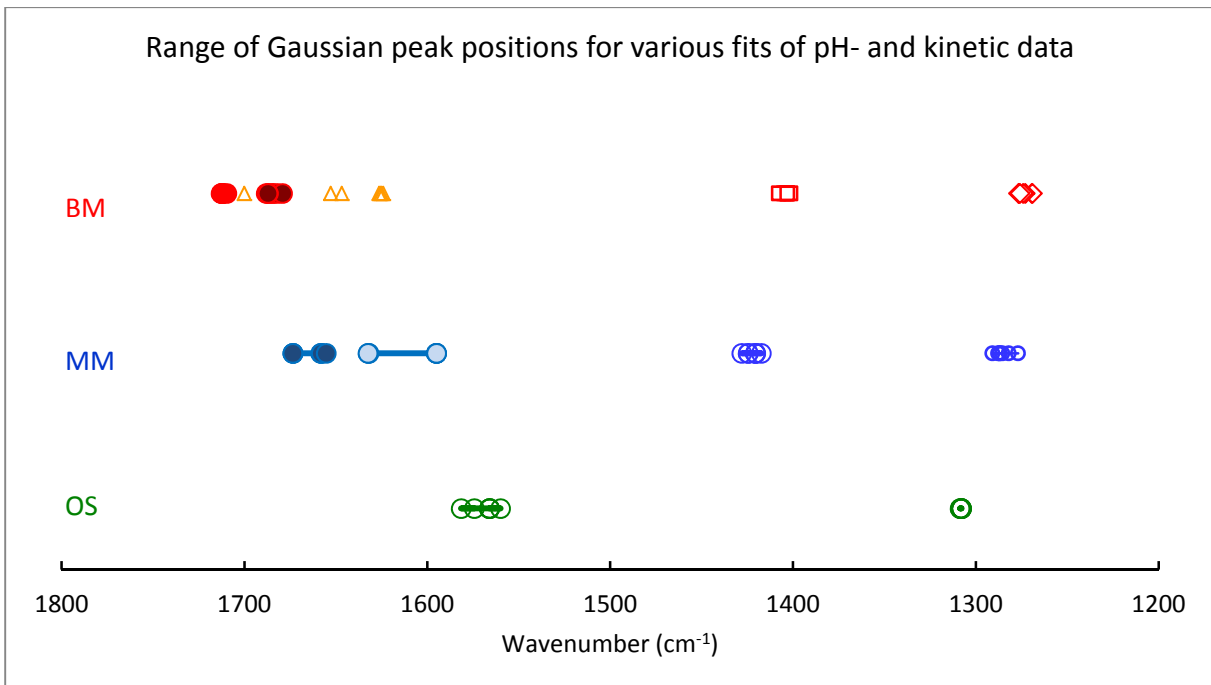


Figure EA7.

Range of peak positions from Gaussian fits to different data sets and subsets of spectra.

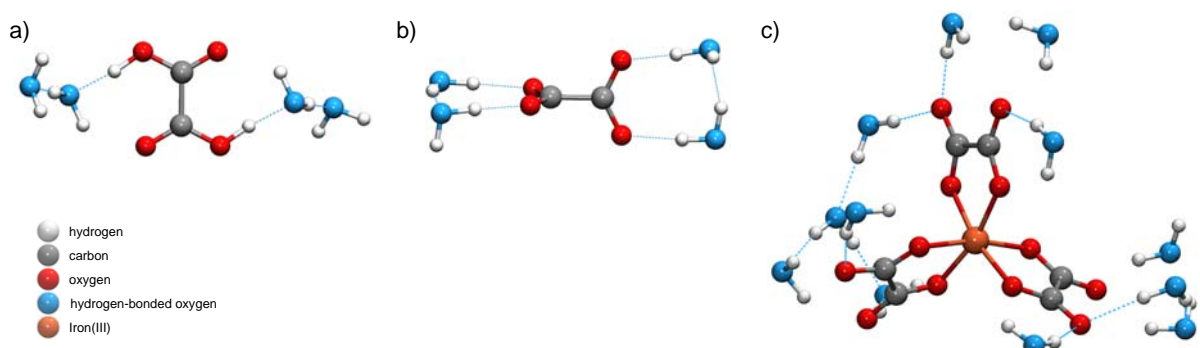


Figure EA8. Molecular clusters of (a) oxalic acid $[\text{H}_2\text{C}_2\text{O}_4 \cdot 4 \text{ H}_2\text{O}]$, (b) oxalate $[\text{C}_2\text{O}_4 \cdot 4 \text{ H}_2\text{O}]^{2-}$, and (c) trisoxalatoiron(III) $[\text{Fe}(\text{C}_2\text{O}_4)_3 \cdot 12 \text{ H}_2\text{O}]^{3-}$. Geometries were optimized at the B3LYP/6-31G(d,p)/PCM(water) level.

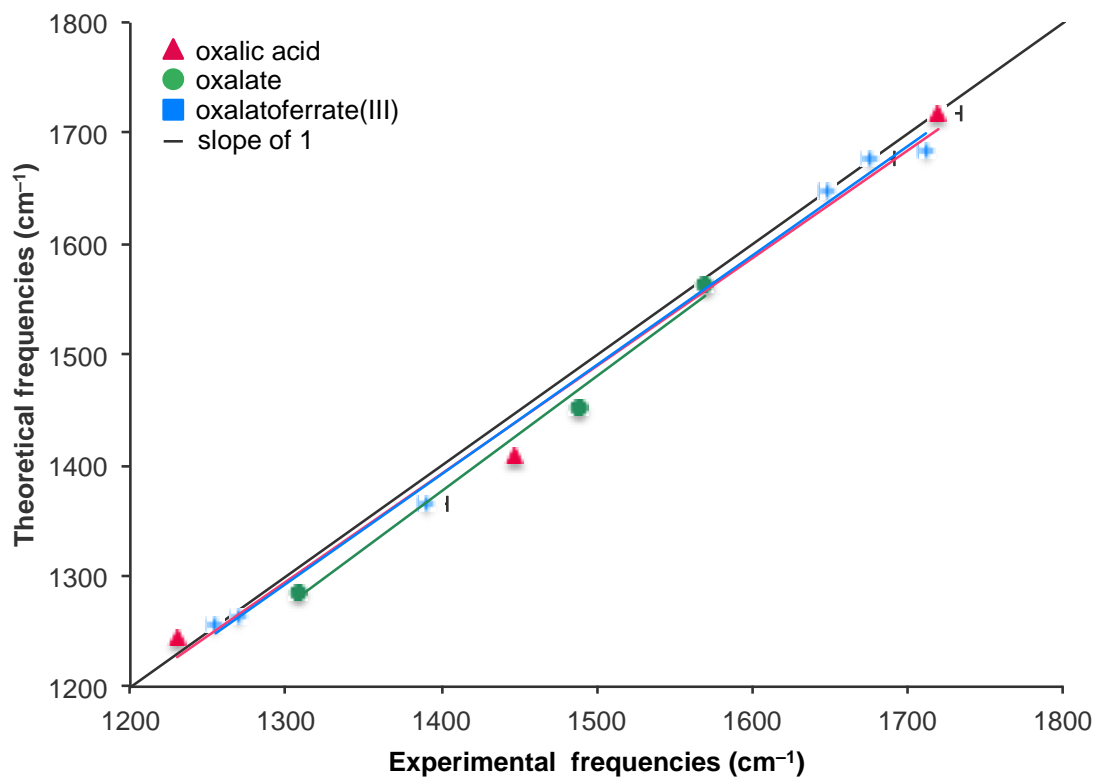


Figure EA9. Linear regression plots that compare experimental and theoretical frequencies of aqueous oxalic acid, oxalate dianion, and oxalato ferrate(III). Linear fit parameters are given in [Table EA 5](#).

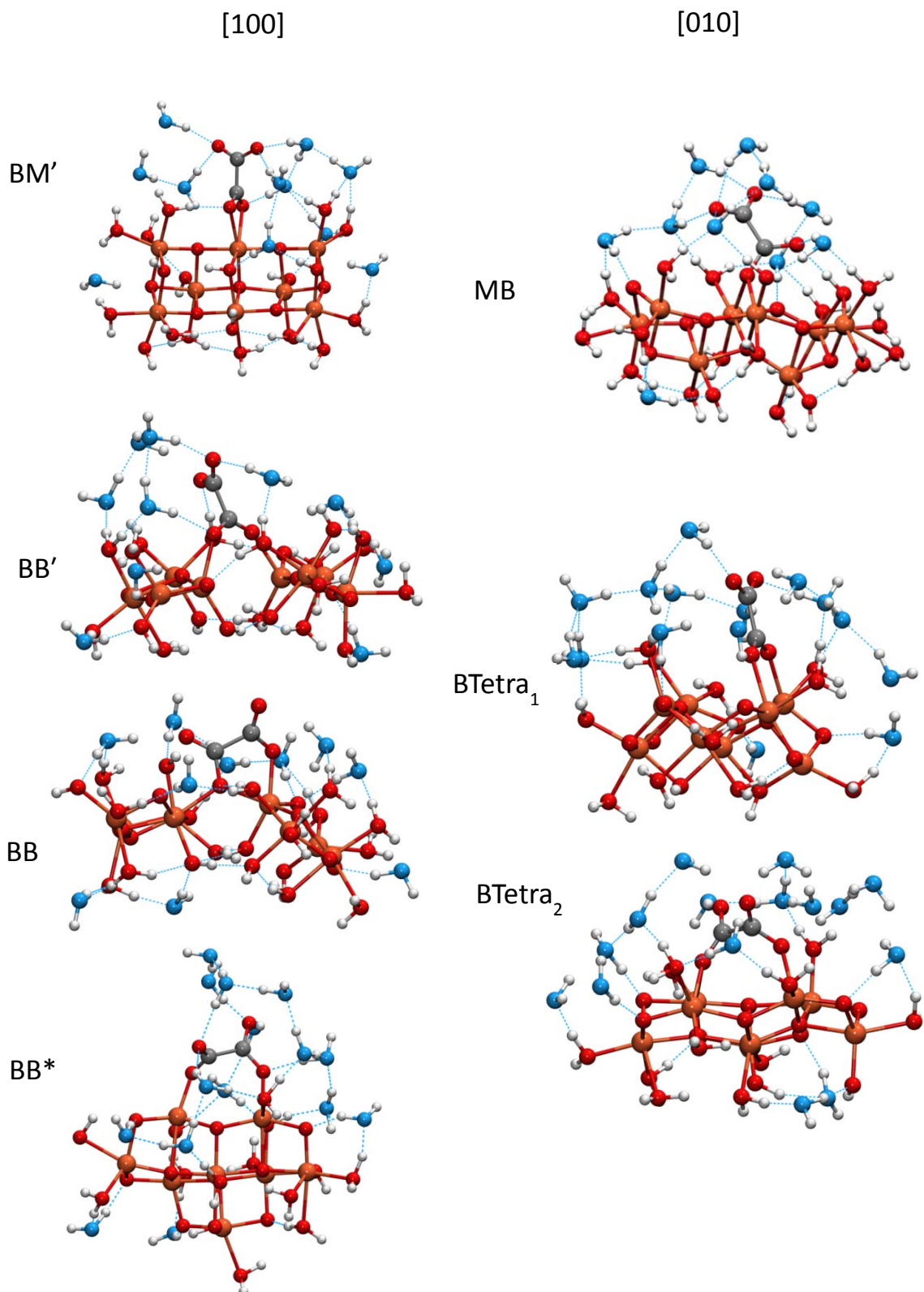


Figure EA10. Geometry-optimized molecular clusters of oxalate adsorbed to lepidocrocite.

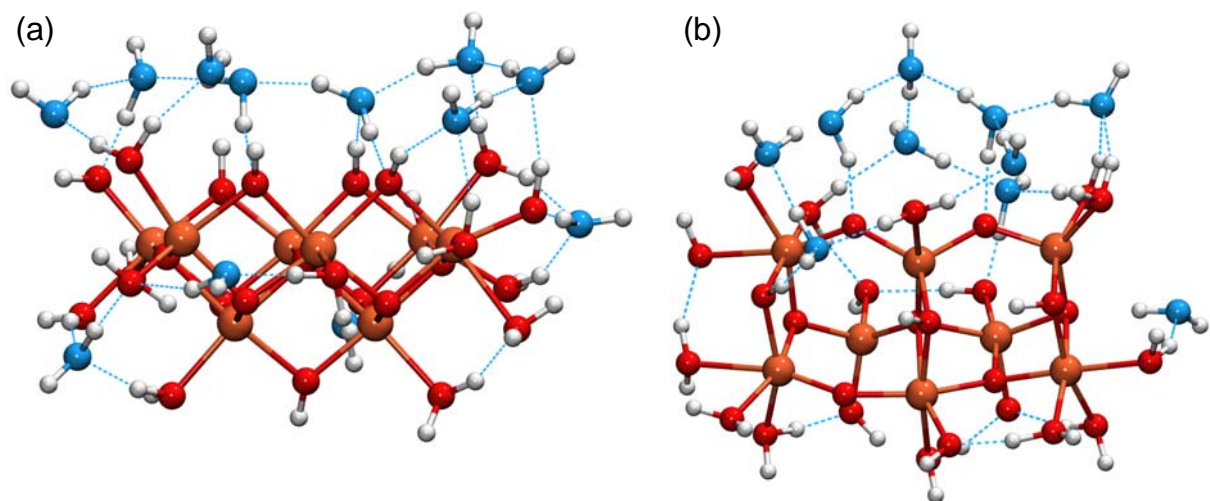


Figure EA11. Geometry-optimized molecular clusters of solvated lepidocrocite cluster $[\text{Fe}_8\text{O}_{38}\text{H}_{54}]^{2+}$, representing (010) and (100) surfaces, respectively.

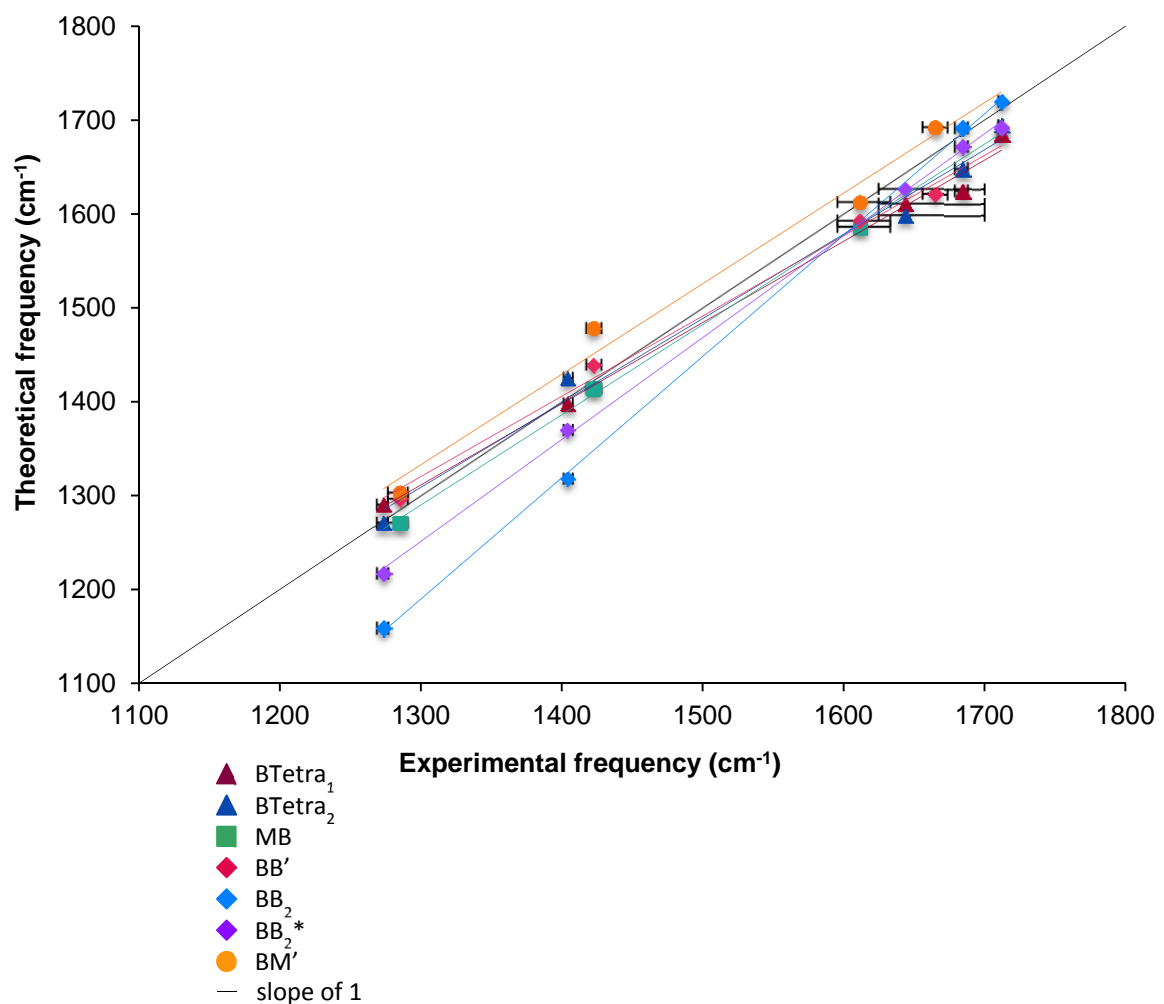


Figure EA12. Linear regression comparison of experimental and theoretical frequencies of molecular clusters modeling inner-sphere bonded complexes. Linear fit parameters are given in [Table EA6](#).

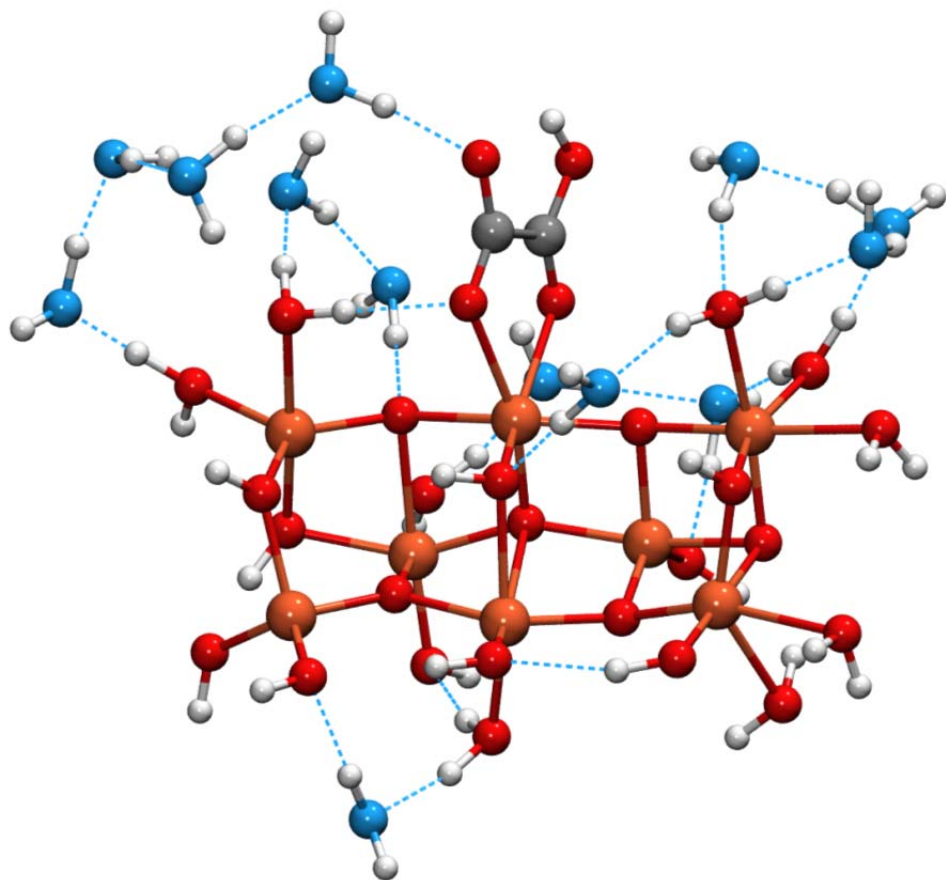


Figure EA13. Geometry-optimized molecular cluster with protonated **BM**.

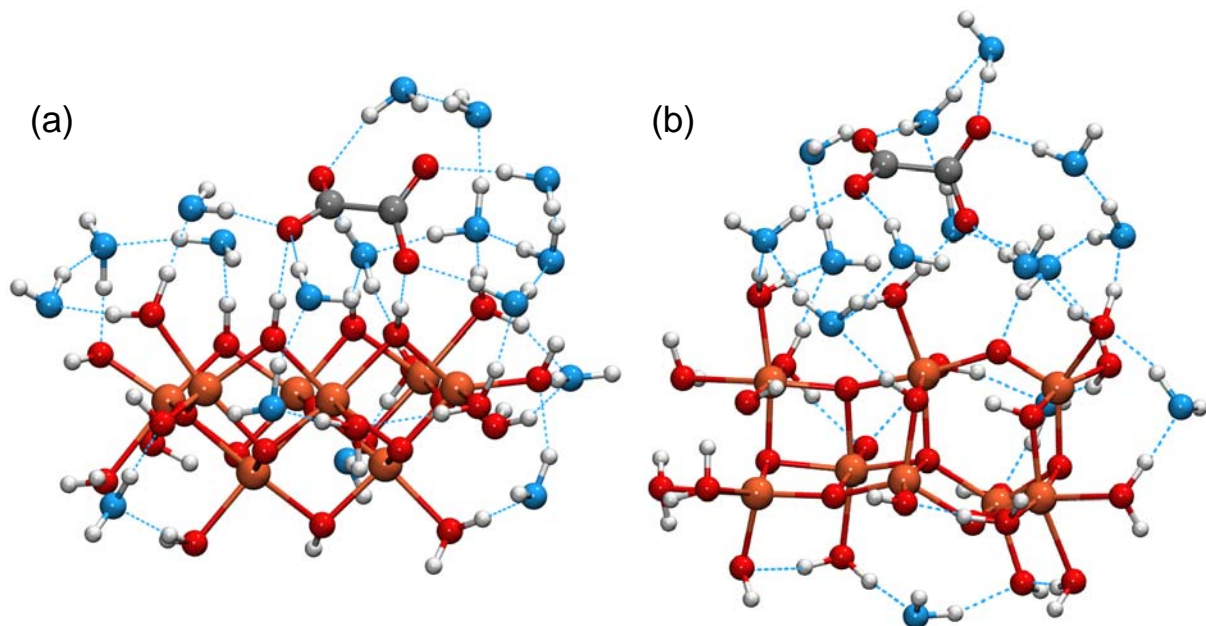


Figure EA14. Geometry-optimized molecular cluster $\mathbf{H}\text{-}\mathbf{OS}_{(010)}$ and $\mathbf{H}\text{-}\mathbf{OS}_{(100)}$.

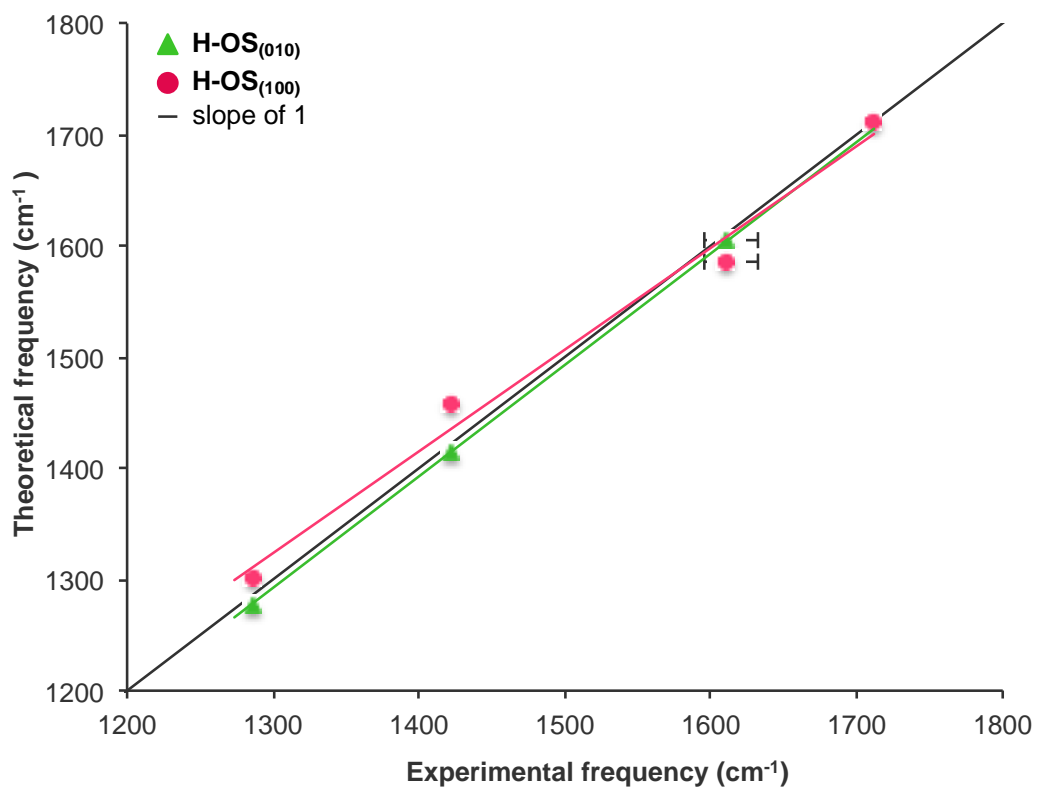


Figure EA15. Linear regression comparison of experimental and theoretical frequencies of $\mathbf{H}\text{-}\mathbf{OS}_{(010)}$ and $\mathbf{H}\text{-}\mathbf{OS}_{(100)}$. Linear fit parameters are given in Table EA3.

References

- Akutsu, H., Akutsu-Sato, A., Turner, S.S., Day, P., Canadell, E., Firth, S., Clark, R.J.H., Yamada, J.I. and Nakatsuji, S. (2004) Superstructures of donor packing arrangements in a series of molecular charge transfer salts. *Chem. Commun.* 10, 18-19.
- Braga, D., Eckert, M., Fraccastoro, M., Maini, L., Grepioni, F., Caneschi, A. and Sessoli, R. (2002) The hydrogen oxalate anion allows one-dimensional columnar aggregation of organometallic sandwich cations. *New Journal of Chemistry* 26, 1280-1286.
- Brill, R., Hermann, C. and Peters, C. (1943) Röntgenographische Fouriersynthese von Oxalsäure-Dihydrat. *Annalen der Physik* 434, 357-377.
- Cornell, R.M. and Schwertmann, U. (2003) *The Iron Oxides: Structure, Properties, Reactions, Occurrences, and Uses*, 2nd ed.; ed. Wiley-VCH, New York, NY, USA.
- Coronado, E., Curreli, S., Giménez-Saiz, C., Gómez-García, C.J. and Alberola, A. (2006) Radical salts of bis(ethylenediseleno)tetrathiafulvalene with paramagnetic tris(oxalato)metalate anions. *Inorganic Chemistry* 45, 10815-10824.
- Fujita, J., Martell, A.E. and Nakamoto, K. (1962) Infrared spectra of metal chelate compounds. VI. A normal coordinate treatment of oxalato metal complexes. *J. Chem. Phys.* 36, 324-331.
- Hind, A.R., Bhargava, S.K., Van Bronswijk, W., Grocott, S.C. and Eyer, S.L. (1998) On the Aqueous Vibrational Spectra of Alkali Metal Oxalates. *Applied Spectroscopy* 52, 683-691.
- Hug, S.J. and Bahnemann, D. (2006) Infrared spectra of oxalate, malonate and succinate adsorbed on the aqueous surface of rutile, anatase and lepidocrocite measured with in situ ATR-FTIR. *J. Electron Spectrosc Relat Phenom* 150, 208-219.
- Martin, A. and Alan Pinkerton, A. (1998) Charge Density Studies Using CCD Detectors: Oxalic Acid at 100 K Revisited. *Acta Crystallographica Section B: Structural Science* 54, 471-477.
- Persson, P. and Axe, K. (2005) Adsorption of oxalate and malonate at the water-goethite interface: Molecular surface speciation from IR spectroscopy. *Geochim. Cosmochim. Acta* 69, 541-552.
- Saritha, A., Raju, B., Ramachary, M., Raghavaiah, P. and Hussain, K.A. (2012) Synthesis, crystal structure and characterization of chiral, three-dimensional anhydrous potassium tris(oxalato)ferrate(III). *Physica B: Condensed Matter* 407, 4208-4213.
- Shippey, T.A. (1980) Vibrational studies in aqueous solutions. *Journal of molecular structure* 65, 71-86.